Cosmic-ray muon fluxes deep underground: Intensity vs depth, and the neutrino-induced component

M. F. Crouch
Department of Physics, Case Western Reserve University, Cleveland, Ohio 44106

P. B. Landecker,* J. F. Lathrop,† F. Reines, W. G. Sandie,‡ and H. W. Sobel
Department of Physics, University of California, Irvine, California 92717

H. Coxell** and J. P. F. Sellschop
Nuclear Physics Research Unit, University of the Witwatersrand, Johannesburg, Transvaal, Republic of South Africa
(Received 3 March 1978; revised manuscript received 12 September 1978)

The angular distribution of muons observed deep underground (10788 ft, or 8.89×10^5 g cm^{-2} standard rock) has been measured with a 174-m^2 liquid scintillation detector in conjunction with 48384 neon flash tubes. The data are fitted by a curve giving the vertical intensity of muons vs vertical depth h_0 as $I_{\nu\mu}(h_0) = A\exp(-h_0/\lambda) + I_{\nu\mu}^{(\nu)}$, where $A = (2.26\pm0.16)\times10^{-6}$ cm^{-2} sec^{-1} sr^{-1}, and $\gamma = (7.58\pm0.09)\times10^4$ g cm^{-2}. The constant term, representing the measured depth-independent flux of muons produced in the surrounding rock by interactions of cosmic-ray neutrinos generated in the earth's atmosphere, has the value $I_{\nu\mu}^{(\nu)} = (2.23\pm0.20)\times10^{-13}$ cm^{-2}sec^{-1}sr^{-1}. This observed flux is in fair agreement with that predicted assuming a cosmic-ray neutrino flux which is a composite of several theoretical estimates. Thus the flux of muons from extraterrestrial neutrinos is $<10^{-13}$cm^{-2} sec^{-1}sr^{-1}.

I. INTRODUCTION

A large-area array of liquid scintillation detectors and flash tubes has been operated deep underground (8.89×10^5 g cm^{-2} standard rock) (from 13 December 1967 to 28 October 1971) to study the intensity and angular distribution of cosmic-ray muons. The depth and array configuration were chosen to permit measurement of the transition from the angular region where penetrating muons produced in the earth's atmosphere predominate (zenith angle $<45^\circ$), to the region where the entire muon flux is neutrino-induced. The familar atmospheric muons and the neutrinos whose interactions we observe are both components of the cosmic rays which reach the earth following the cascade of interactions that occur when primary cosmic rays enter the earth's atmosphere.[1]

Our basic motivation for this study is to investigate the weak interaction in the high-energy region. Measurement of the muon flux deep underground provides a test of the correctness of the theory of the $\nu_\mu+\bar{\nu}_\mu$ processes producing muons (charge-changing ν_μ interaction) which occur in the rock. In addition, the atmospheric neutrino flux represents an important component of the cosmic radiation which should be studied to complete our understanding of cosmic rays as an observed geophysical phenomenon.

Equation (1) shows the two-component nature of the underground muon flux observed at a vertical depth h_0 and at zenith angle θ. $I_\mu^{(\nu)}$ is the flux of muons due to neutrinos, $I_\mu^{(\mu)}$ denotes the flux of atmospheric muons, and h and v denote horizontal and vertical.

$$I_\mu(h_0,\theta) = I_\mu^{(\mu)}(h_0,\theta) + I_\mu^{(\nu)}(\theta)\,, \tag{1}$$

where, assuming that the exponential form of muon absorption extends to these depths,

$$I_\mu^{(\mu)}(h_0,\theta) = I_{v\mu}^{(\mu)}(h_0)\,j_\mu(h_0,\theta)\,,$$
$$= (A e^{-h_0/\lambda})\{\sec\theta\exp[(1-\sec\theta)h_0/\lambda]\}\,, \tag{1a}$$

$$I_\mu^{(\nu)}(\theta) = I_{h\mu}^{(\nu)} j_\nu(\theta)\,. \tag{1b}$$

The angular distribution $j_\nu(\theta)$ for the neutrinos $(\nu_\mu+\bar{\nu}_\mu)$ and the muons which they produce has been calculated by Osborne, Said, and Wolfendale.[2] This distribution peaks in the horizontal direction, exhibiting a horizontal-to-vertical ratio of approximately 2/1 when averaged over the energy spectrum (see Fig. 12). The angular distribution for atmospheric muons deep underground [Eq. (1a)] is seen to be very different, being strongly peaked in the vertical direction (cf. Miyake[3]). Accordingly, the data from our observations, analyzed by a maximum-likelihood procedure, permit us to determine the intensities of cosmic-ray muons $I_{v\mu}^{(\mu)}(h)$ and the neutrino-produced muons $I_{h\mu}^{(\nu)}$, as well as the attenuation length λ. The angular measurements at a vertical depth $h_0 = 8.89\times10^5$ g cm^{-2} enable us to infer the vertical intensity of atmospheric muons to the depth 15×10^5 g cm^{-2} at which they become masked by ν-produced muons. Beyond this depth the present observations of the neutrino-induced muon flux

can be used to normalize the calculated angular distribution to yield the flux of produced muons at any depth.

As a final step in the analysis of our data, we use the measured flux of depth-independent muons produced in the rock target surrounding the detector[4] to make deductions regarding the cosmic-ray neutrino flux and cross sections for the interactions

$$(\nu_\mu, \bar{\nu}_\mu) + N \rightarrow (\mu^-, \mu^+) + N' + \cdots . \quad (2)$$

II. THE UNDERGROUND LABORATORY SITE

In order to reduce the atmospheric muon flux so that the neutrino-produced muons can be observed, the apparatus was operated at a depth of 3288 meters below the surface of the earth in East Rand Proprietary Mine (ERPM), near Johannesburg, South Africa. A special tunnel was excavated at some distance from the gold-bearing reef to accommodate our detectors. Earlier experiments of Reines *et al.*[5] and Krishnaswamy *et al.*[6] at lesser depths had already demonstrated the feasibility of studying cosmic-ray neutrino interactions with large-area scintillation detectors. ERPM is a particularly suitable site for muon-flux measurements for the following reasons:

1. The depth available at ERPM [$(8.89 \pm 0.08) \times 10^5$ g cm^{-2}] is preeminently suitable in reducing the atmospheric muon flux to acceptable levels relative to the flux of neutrino-produced muons.

2. The geology of the area has been studied extensively. The rock lying over the site is quartzitic "standard rock," with $\rho = 2.713 \pm 0.007$ g cm^{-2}, $Z/A = 0.499 \pm 0.001$, and $Z^2/A = 5.53 \pm 0.01$.

3. The surface terrain is very flat, making it unnecessary to estimate effective depths for individual events from angular coordinates of particle trajectories and surface topography. Specifically, for muons reaching our detector throughout the range of zenith angles $0 < \theta < 45°$, topographical irregularities cause an additional uncertainty in depth of only ± 6000 g cm^{-2}.

III. APPARATUS

A. Scintillation-detector array

The scintillation-detector array (Figs. 1 and 2) consists of 20 three-segment liquid-scintillation-counter "bays," aggregating 174 m^2 area. Eight of the bays are arranged in a "double-rail" configuration to permit comparison of results with those of the earlier measurement by Reines *et al.*[5] using scintillation detectors only. The remaining 12 bays form a single "rail" to give the largest possible detector aperture, the addition of the flash-tube layers (Fig. 2) providing the necessary directional information for the muons. The scintillation detectors provide the triggering signal required for the flash-tube array.

A detailed description of the elements of the scintillation-counter bay has been given by Reines *et al.*[5] and Crouch *et al.*[7] Figure 2 repeats some of the salient features for clarity. As in the earli-

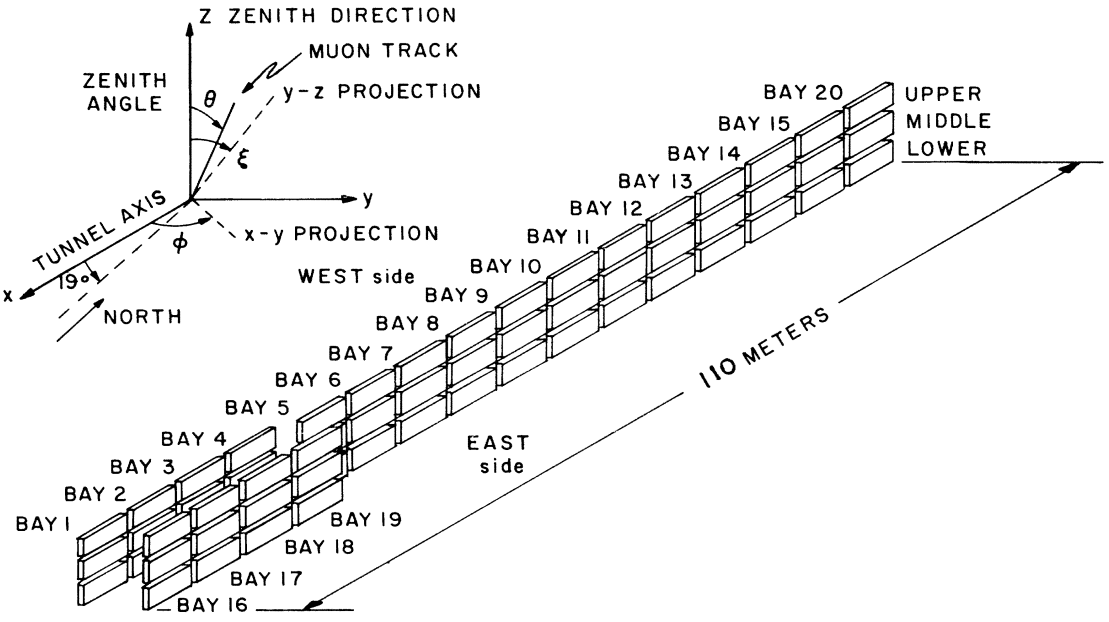

FIG. 1. The scintillation-detector array and the angular coordinate system.

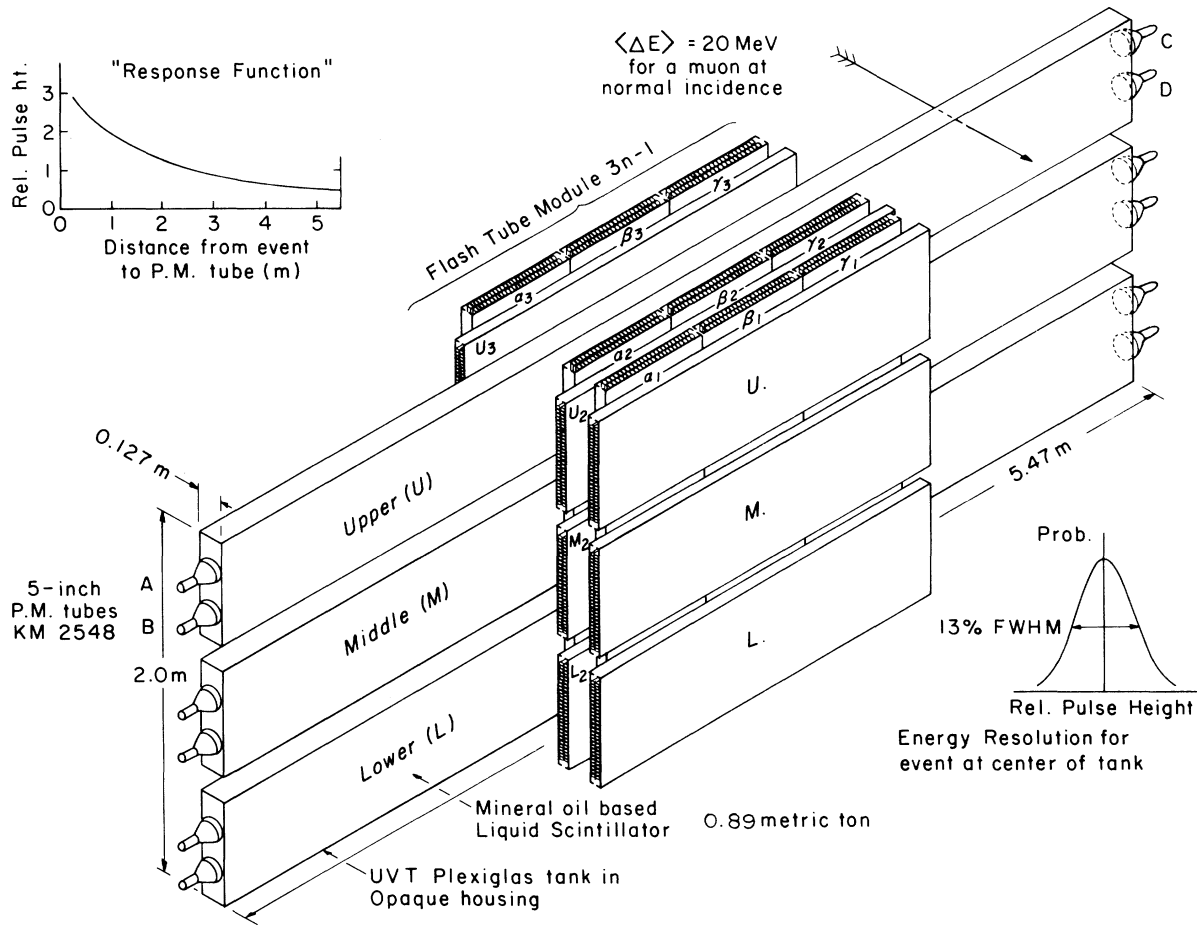

FIG. 2. Details of the nth scintillator bay and the $(3n-1)$st flash-tube module.

er experiment, pulse-height information gives both energy deposition and position of the event to within ±0.15 m along the 5.5-m detector-element length for single-particle events. Figure 3 shows how the scintillation-detector array signals are combined and analyzed to generate a trigger at threshold energy (12 MeV for an event normal to the side of the tank at the center of a bay, 10 MeV for the double-rail array, reflecting a slight difference in the design). Because of the scintillator "response function", Fig. 2, the threshold energy is approximately doubled for muons entering the end regions of a bay. All pulses required to generate a master trigger must arrive in a 1-μsec time interval. Figure 4 shows the variation of triggering probability vs energy deposited by a muon averaged over event position. It is apparent from these figures that a substantial fraction (~80%) of muons which traverse the detector will produce triggers. The underground tanks were calibrated using a muon telescope and an identical tank on the surface of the earth. A portable scintillation detector, a 3C45 thyratron light pulser and a ^{208}Tl radioactive source were used as a part of this secondary standard system to convey the calibration information to the underground array of tanks.

As in our earlier work,[5] data are recorded photographically in analog form, to permit us to clearly distinguish the proper scintillation-detector waveforms appearing on the cathode-ray oscilloscopes from those caused by spurious electrical signals. Figure 5 shows the pulse-position code used to indicate the address of a signal, together with a typical event. The pulses on traces 2 and 4 show the occurrence of the basic fourfold coincidence $A \circ B \cdot C \circ D$ given by the four photomultipliers at the ends of an individual scintillation detector. Different pulse positions are provided for signals from upper (U), middle (M), or lower (L) segments. The bay location is determined by grouping the analog signals according to the 4×5 matrix scheme shown in Fig. 3. Two "locator" pulses in the display denote, respectively, row and column in the matrix, thus uniquely specifying the bay number. If more than two loca-

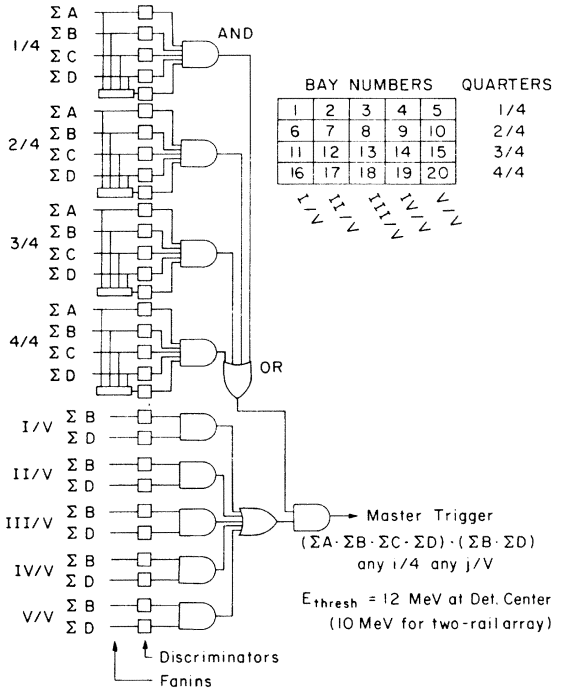

FIG. 3. Logic circuits for triggering the scintillation-detector array.

tor pulses are displayed, the event is either spurious (i.e., chance near-simultaneous γ-ray signals near the ends of two detector elements), or complex in nature (i.e., a shower) and it is possible to interpret these correctly following detailed analysis, especially given complete flash-tube system data. Spurious signals from γ rays are ordinarily too small to be consistent with a real event involving more than one scintillation detector, and are not accompanied by any flash-tube system tracks. A system of three mutually

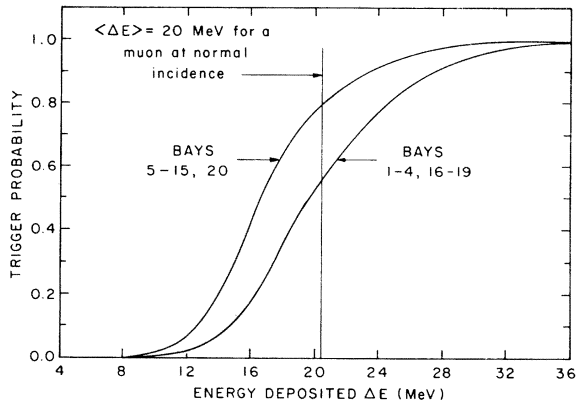

FIG. 4. Triggering probability for the scintillation-detector array vs energy deposition.

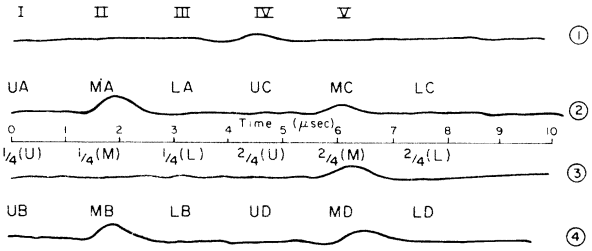

First-Half Chronotron Display: Event No. 205 - BAY 9, Middle Tank.

FIG. 5. Pulse-position code for scintillation-detector signals, showing a representative event—event No. 205, middle detector, bay 9.

perpendicular geophones was used to exclude the relatively rare false events due to mechanical motion associated with seismic activity.

B. Flash-tube array

A modular system of flash tubes is used to record the particle trajectories. Figures 2 and 6 show some of the details of this system.[8] 56 flash tubes in two layers enclosed in an electrode structure comprise an "element" of sensitive area 0.5 m×2.0 m. Figure 2 shows how 18 of these elements are combined to form a "module" giving six horizontal layers and six vertical layers extending over a region of $\frac{1}{3}$ bay. A double-rail section is identical except for the addition of a second scintillation rail. Two additional modules complete the coverage for one bay, actually extending slightly beyond the ends of the bay. 48 of these modules, aggregating 48 384 flash tubes, comprise the full array. Because the array fills a mine tunnel for a distance of more than 100 meters, the usual photographic recording of the flash-tube discharges is not readily accomplished. Consequently, as shown in Fig. 6, the flat end of each flash tube is provided with a light sensor (a cadmium selenide photoresistive cell) and a thyristor latch circuit to store and display the pattern of optical discharges. A multiplexed readout circuit with 972 incandescent lamps and 972 current lines is used with a three-level logic circuit to display sequentially the stored flash-tube information from nine modules straddling the region where the scintillation-detector signal is sensed. The nine conformally mapped flash-tube displays are recorded with a 35-mm camera.

The selector signals to store the flash-tube displays in the appropriate portion of the array are generated by an extension of the scintillation-detector triggering logic described in Fig. 3. A simple decoder circuit converts the row and column data in the 4×5 matrix to 20 bay lines.

The flash tubes are glass tubes 2.0 m long, with

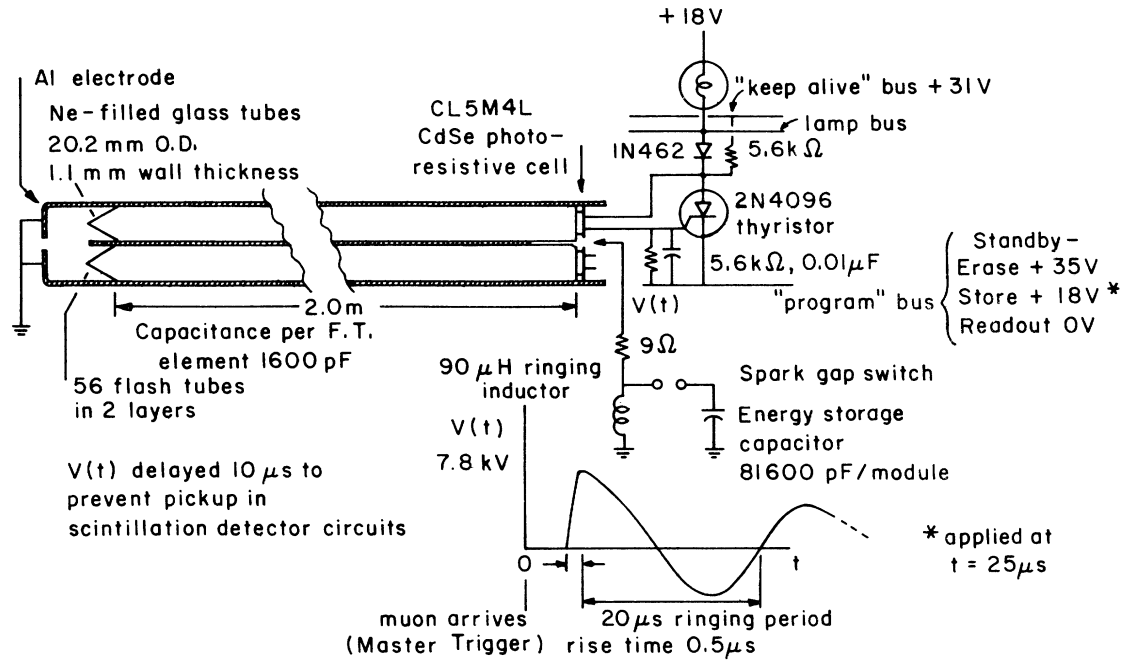

FIG. 6. Flash-tube element and associated circuits.

outside diameter 17.5 mm, wall thickness 1.1 mm,[9] filled with neon to a pressure of 60 mm Hg. The "layer efficiency," for muons incident normally on a single layer of close-packed flash tubes is

$$\frac{(17.5/2)-1.1-\delta}{17.5/2}=0.86\,.$$

The quantity $17.5/2-1.1-\delta$, where δ is a small quantity experimentally determined to be ~0.125 mm, is the effective radius within which a traversing muon will produce detectable ionization. The bipolar high-voltage pulse is believed to reduce the effects of the built-in clearing field and thus maximizes the layer efficiency. More important for the analysis of our data is the probability of observing a flash in both layers of a flash-tube element, as the projected angle of incidence ξ (or φ), Fig. 1, is varied. Figure 7 shows this probability $P_2(\xi)$ calculated for our elements, together with the experimentally measured values. At $\xi=90^\circ$ (normal incidence), $P_2(\xi)$ approaches the layer efficiency, since the inert wall regions of two ideally aligned layers act in concert. At $\xi \cong 80^\circ$, the inert wall regions of the two layers act separately to prevent flashes in one layer or the other, so giving a lowered efficiency $P_2(\xi)$. However, for $\xi \lesssim 60^\circ$, it is impossible to draw a muon trajectory through the double layer that does not pass through the sensitive region of one or more flash tubes on each side, whereupon $P_2(\xi)=1.0$. It is seen that experimentally measured values of $P_2(\xi)$ are in fair agreement with expected values, though it is significant that the measured values tend to be systematically low.

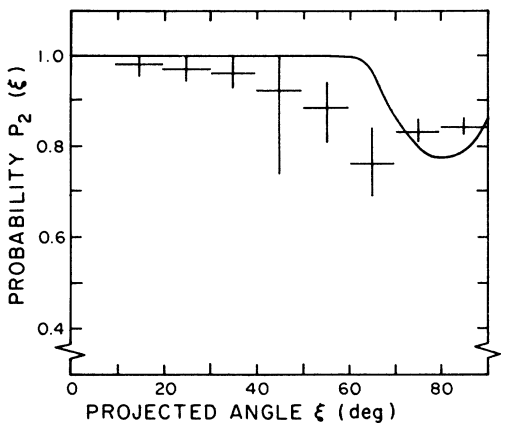

FIG. 7. Probability $P_2(\xi)$ of a two-layer response in a flash-tube element vs projected angle ξ for horizontal flash tubes or φ for vertical tubes.

Despite the large number of flash tubes used, and the placement of them in the optimum positions to observe the generally horizontal muon tracks of principal interest, the planes of flash tubes still contain numerous gaps which lead to missed tracks in the horizontal and/or vertical flash-tube planes (see Appendix B). As a result one or both of the stereoscopic views of the track are missing for some events, making it impossible to determine the muon's zenith angle. Several interesting events in this category with incomplete

data on the muon trajectory have such a complex nature that it is impossible to reconstruct the event in detail. Fortunately it is possible to calculate the aperture of the array for muons in all ranges of zenith angle, including those which miss part or all of the flash-tube array. Thus the various classes of observed rates (six in all) can be compared with corresponding expected rates to determine the parameters A, λ, and $I_{\mu}^{(\nu)}$ in Eq. (1).

It should be noted that inspection of the flash-tube data reveals somewhat more frequent events with incomplete tracks than would be expected from the calculated aperture and efficiency values. From a study of the behavior of the likelihood function it appears reasonable to explain this by an "excess inefficiency" (~16%) which accommodates periods when portions of the large and complex flash-tube array were inoperative and even brief periods when problems such as high humidity have caused the entire system to fail.[10] As described in Appendix A it is possible to correct the calculated differential array apertures to take account of the effect of this moderate excess inefficiency.

IV. ANALYSIS OF THE MUON-FLUX DATA

As noted in the introduction, the muon flux we observe consists of two very distinctly different components. Muons from neutrino interactions in the rock surrounding the detector array are peaked in the horizontal direction. The atmospheric muons which penetrate the earth to our depth are very sharply peaked in the vertical direction. The histogram of Fig. 8, which shows the observed angular distribution of muons studied with our flash-tube array, clearly demonstrates the presence of these two components.[11] A maximum-likelihood calculation applied to these data together with other classes of data for which the flash-tube array gives incomplete information on the muon's path, permits us to determine the parameters $I_{\nu\mu}^{(\mu)}(h)$, λ, and $I_{\nu\mu}^{(\nu)}$ which quantitatively characterize these two components. The angular distribution $I_{\mu}^{(\nu)}(\theta)$ for neutrino-produced muons assumed in these calculations is that given by Osborne, Said, and Wolfendale[2] for 10-GeV neutrinos. However, as shown in Reines *et al.*[5] the result is insensitive to the assumed form over the range of angular distributions given by Osborne *et al.* for various values of neutrino energy.

For n categories of events, the likelihood that the observed numbers of events will be N_1, $N_2, \ldots, N_n$, when $C_1, C_2, \ldots, C_n$ are the expected numbers of events, is given by the Poisson expression

$$L = \prod_{i=1}^{n} \frac{C_i^{N_i} e^{-C_i}}{N_i!}, \tag{3}$$

where

$$C_i = t_i \int_{\theta=0}^{\pi} I_{\mu}(h_0, \theta) \frac{dA_i}{d\theta} d\theta . \tag{4}$$

Here t_i is the sensitive time, $I_{\mu}(h_0, \theta)$ is the composite muon intensity given in detail in Eq. (1), and $dA_i/d\theta$ are the differential apertures for the array in $\mathrm{cm}^2\,\mathrm{sr}^{-1}\,\mathrm{rad}^{-1}$. The latter are discussed in Appendix A, together with analytic calculations of the corrections for "excess inefficiency." Using standard statistical techniques,[12] an iterative computer program is used to search for the condition that this Poisson likelihood function has its maximum value, whereupon the parameters sought

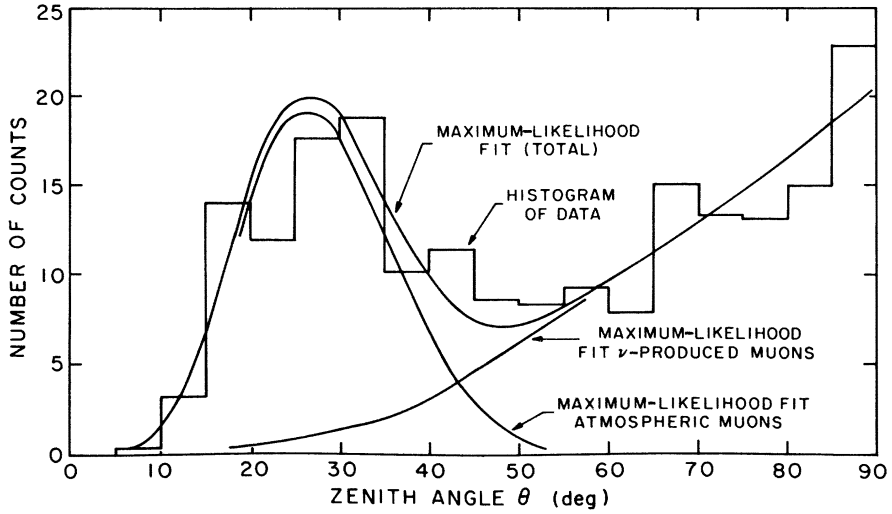

FIG. 8. Observed and expected numbers of counts vs zenith angle for events in which zenith angle is determined.

TABLE I. Results of maximum-likelihood calculation.

$A = (2.26 \pm 0.16) \times 10^{-6}\ \mathrm{cm^{-2}\,sec^{-1}\,sr^{-1}}$

$\lambda = (7.58 \pm 0.09) \times 10^{4}\ \mathrm{g\,cm^{-2}}$ [a]

$I_{v\mu}^{(\mu)} = (1.82 \pm 0.13) \times 10^{-11}\ \mathrm{cm^{-2}\,sec^{-1}\,sr^{-1}}$

$I_{v\mu}^{(\nu)} = (2.23 \pm 0.20) \times 10^{-13}\ \mathrm{cm^{-2}\,sec^{-1}\,sr^{-1}}$

$I_{h\mu}^{(\nu)} = (4.59 \pm 0.42) \times 10^{-13}\ \mathrm{cm^{-2}\,sec^{-1}\,sr^{-1}}$

Zenith angle θ (deg)	Observed counts N_i	Expected counts C_i
10–15	3.2	3.9
15–20	14.0	10.7
20–25	11.9	18.3
25–30	17.7	20.0
30–35	18.8	16.6
35–40	10.1	11.9
40–45	11.4	8.3
45–50	8.6	7.1
50–55	8.4	7.6
55–60	9.2	8.8
60–65	7.8	10.4
65–70	15.1	12.0
70–75	13.3	13.8
75–80	13.1	15.6
80–85	15.0	17.8
85–90	22.9	19.6
Total	200.5	202.4
Projected zenith angle only	41	40.7
Azimuth angle only	38	50.9
No track in flash-tube data	107	89.5
IVA (U and M, or M and L) [b]	51	53.6
IVB (U and M and L) [b]	12	12.2
Total	249	246.9
Event grand total	449.5	449.3

[a] Includes ±0.9% uncertainty in depth.
[b] Events furnishing scintillator signal only.

and their standard deviations are determined. Table I and Figs. 8 and 9 give the results of the maximum-likelihood calculation and show the values of C_i and N_i, the expected and observed numbers of events, in the various data categories.

Figure 9 indicates the depth (1.3×10^6 g cm^{-2}, standard rock) at which the vertical flux of muons from the atmosphere equals that of muons from the interaction of atmospherically produced neutrinos. Beyond this "ultimate" depth, neutrino-produced muons predominate at all angles so that measurements of the muon depth-intensity curve cannot be used to deduce the atmospheric muon spectrum for muon energies $\gtrsim 4 \times 10^4$ GeV.[13]

It is worth remarking that the likelihood function when 16% excess-inefficiency correction is assumed, is greater than that for the uncorrected data by a factor of over 5000.

V. THE FLUX OF COSMIC-RAY NEUTRINOS

We next consider the interrelationship of the observed horizontal neutrino-induced component of the muon flux $I_{h\mu}^{(\nu)}$ with the interaction cross sections, the size of target, and the neutrino, antineutrino flux. Equation (5) details this relationship:

$$I_{h\mu}^{(\nu)} = \int \left[I_{h\nu}(E_\nu)\sigma_\nu(E_\nu) + I_{h\bar{\nu}}(E_\nu)\sigma_{\bar{\nu}}(E_\nu) \right] \times N_A R(kE_\nu) dE_\nu \,. \quad (5)$$

(a) $I_{h\nu}$, $I_{h\bar{\nu}}$ are the horizontal fluxes of neutrinos and antineutrinos, which are functions of the neutrino, antineutrino energy E_ν. Figure 10 shows assumed values for these fluxes. For the energy range 0.1 GeV (threshold energy) $\leq E_\nu \leq 10$ GeV, calculations of Young[14] made for latitude 26°S, the

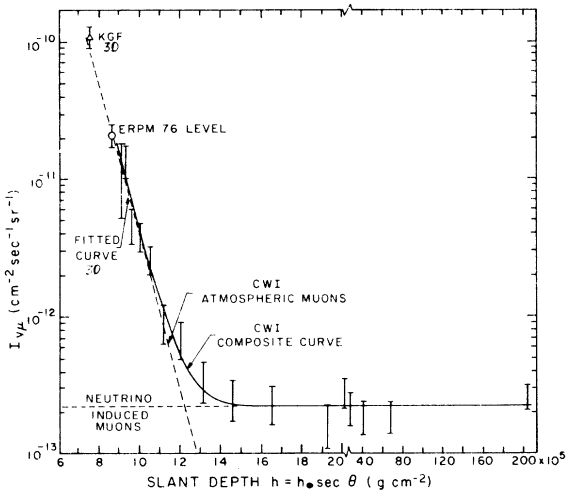

FIG. 9. Vertical intensity $I_{v\mu}$ of muons vs slant depth h, deduced from muon angular distribution at $h_0 = 8.89 \times 10^5$ g cm^{-2}. Fitted curve is from Ref. 30.

location of Johannesburg, are used. For the range $10 \leq E_\nu \leq 1000$ GeV, the $\nu + \bar{\nu}$ flux calculated by Osborne, Said, and Wolfendale[2] is used, combined with the $\nu/\bar{\nu}$ ratios given by Pal.[15] For the range 1000 GeV $\leq E_\nu \leq 10$ TeV an extrapolation of the flux values is made which approximately maintains the same rate of steepening of the spectra. Since the contribution in this range is small, the results are relatively insensitive to the precise form of the extrapolation.

(b) $\sigma_\nu, \sigma_{\bar{\nu}}$ are the total charged-current interaction cross sections for muon neutrinos and antineutrinos. Over the energy range $E_\nu > 60$ GeV, the cross sections used are $\sigma_\nu = 0.61 E_\nu \times 10^{-38}$ cm^2/nucleon and $\sigma_{\bar{\nu}} = 0.29 E_\nu \times 10^{-38}$ cm^2/nucleon, where E_ν is the neutrino, antineutrino energy in GeV.[16] Over the range $2.5 < E_\nu < 10$ GeV the cross sections used are $\sigma_\nu = 0.74 E_\nu \times 10^{-38}$ cm^2/nucleon and $\sigma_{\bar{\nu}} = 0.28 E_\nu \times 10^{-38}$ cm^2/nucleon. Between the threshold energy 0.1 GeV and 2.5 GeV, these expressions are modified to represent the cross section in this region as described by Chen *et al.*[17] Between 10 and 60 GeV, we used a smooth transitional curve matching the two sets of measured values.

(c) The factor N_A (Avogadro's number) gives the number of target nucleons per gram of rock.

(d) $R(kE_\nu)$ is the range of the product muon in the rock, in units of g cm^{-2} where k represents the fraction of the neutrino energy E_ν imparted to

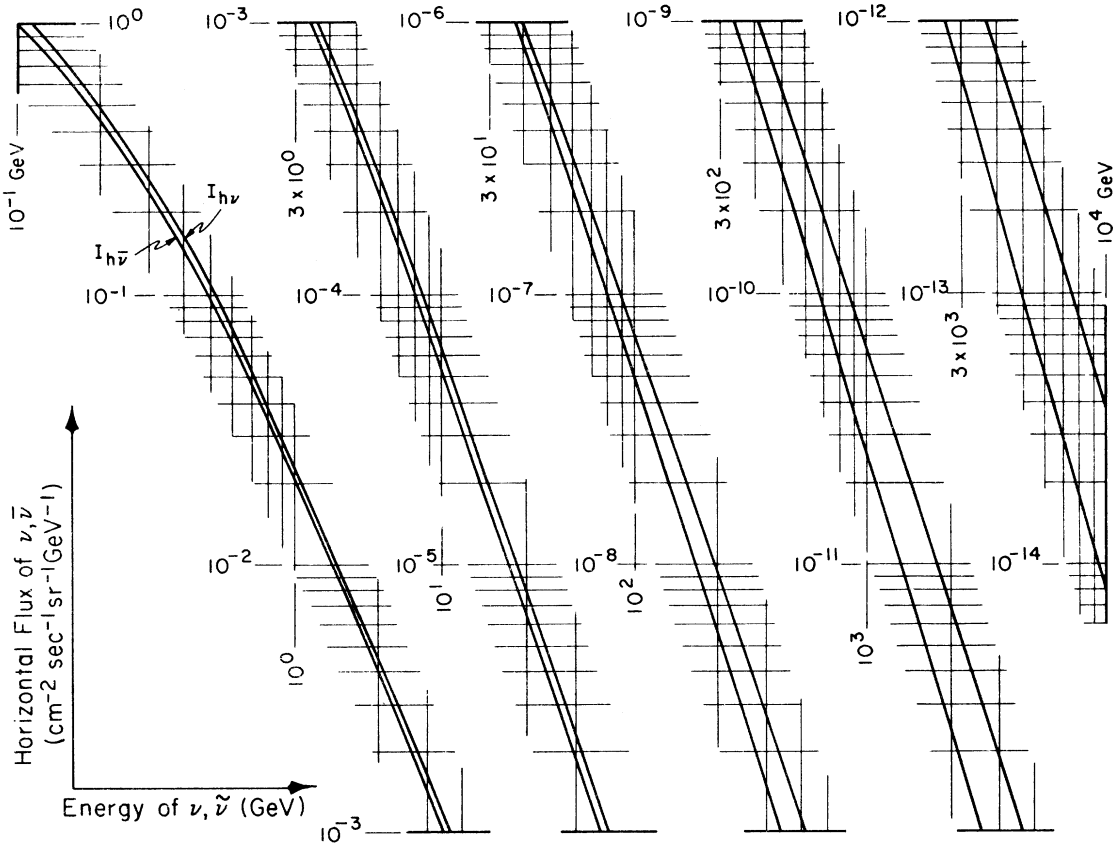

FIG. 10. Horizontal flux for cosmic-ray muon neutrinos, muon antineutrinos.

TABLE II. Expected neutrino-induced muon flux in the horizontal direction, calculated from Eq. (5). The observed neutrino-induced muon flux in the horizontal direction is $I_{h\mu}^{(\nu)}=(4.59\pm0.42)\times10^{-13}$ cm^{-2} sec^{-1} sr^{-1}.

Energy range (GeV)	Contributions to $I_{h\mu}^{(\nu)}$, using Eq. (5) (units of 10^{-13} sec^{-1} cm^{-2} sr^{-1})
0.1 to 1	0.5
1 to 10	2.0
10 to 100	2.4
100 to 1000	1.8
1000 to 10^4	0.8
Total expected flux for range $0.1\leq E\leq10^4$	7.5×10^{-13}

the muon. The range-energy curve of Menon and Ramana Murthy for muons in standard rock is used.[18] Data from accelerators determine k values[19] for energies from 30–200 GeV. For ν_μ, $k=0.53$; for $\bar{\nu}$, $k=0.68$.

Electrons contribute only about 4% to the calculated rate, primarily because the range of the electron is so much less than the muon range in the energy interval of interest.

Table II shows the results of the evaluation of the integral in Eq. (5). The integral is evaluated to an upper limit of $E_\nu=10^4$ GeV, beyond which the flux and cross-section values are not well known but where the contribution to the integral is small. Chen *et al.*[17] assumed saturation of the cross section in the high-energy region via a "propagator" with a range of boson-mass values from $M_W=1.8$ Gev/c^2 to a limit of 1000 GeV/c^2 at which negligible saturation occurs. The present experimental lower limit on the boson mass obtained with accelerators[20] is 30 GeV/c^2, a number to be compared with a theoretically[21] expected 70 GeV/c^2. An assumed M_W of 70 GeV/c^2 would lower cross sections at $E_\nu=10^3$ GeV by about 25%, but would make a relatively small correction to the value of the integral given in Table II.

We conclude that there is fair agreement between the total observed and expected neutrino-induced muon flux (Table II), i.e.,

$$\frac{I_{h\mu}^{(\nu)}(\text{predicted})}{I_{h\mu}^{(\nu)}(\text{observed})}=1.6\pm0.4\ .$$

The uncertainty arises from the neutrino fluxes (±30% for $0.1<E<10$ GeV, with somewhat less imprecise values for $E>10$ GeV), extrapolation of the cross sections beyond the measured region (i.e., >200 GeV) and in the range of the product muon.

Since the observed neutrino-induced muon flux appears to be approximately equal to the expected value,[22] the limit on the muon flux due to neutrinos of extraterrestrial origin is taken to be 20% of the observed horizontal muon flux or $<10^{-13}$ cm^{-2}sec^{-1}sr^{-1} for a neutrino spectrum of the same shape as the atmospheric neutrino spectrum.[23,24]

Further evidence for the predominantly atmospheric origin of the observed flux is the generally uniform distribution of events in celestial coordinates. There is also no directional correlation of events coming from the sun or to local standard time. Several events with very high energy deposition in the scintillation detectors (400–500 MeV) were observed. In each case the flash-tube system indicated that the event consisted of a shower of many particles, so ruling out their interpretation in terms of magnetic monopoles.

ACKNOWLEDGMENTS

This research was supported in part by the United States Department of Energy. G. H. Muller and J. P. H. Tibbles were most helpful in the installation and maintenance of the underground array. G. Nelson played an important role in scanning the film records. D. Bourne and D. Kramers helped with the analysis of the data. The cooperation of the management and staff of the East Rand Proprietary Mines is gratefully noted as is the support of the South African Chamber of Mines. Robert W. Brown has given helpful advice regarding the analysis of the data. H. S. Gurr helped in the design of the logic circuits. A special word of appreciation is due our engineer, A. A. Hruschka, for his vital part in the design, construction, and installation of the underground laboratory.

APPENDIX A

CALCULATION OF DETECTOR APERTURES

A computer code has been developed which, although reminiscent of the numerical calculation of Meyer *et al.*,[25,26] is considerably more general in scope, to accommodate the flash-tube system.

Differential apertures $dA_{i;j,k}/d\theta$, for scintillation-detector classification i, and flash-tube classification j,k are defined as

$$\frac{dA_{i;j,k}}{d\theta}=\int\oint\oint_s \epsilon_{i;j,k}(\vec{\omega},\vec{s})\frac{d\vec{\omega}}{d\theta}\cdot d\vec{s}\,, \qquad \text{(A1)}$$

where $d\vec{s}$ is an element of detector surface area and $\epsilon_{i;j,k}(\vec{\omega},\vec{s})\,d\vec{\omega}\cdot d\vec{s}$ is the probability that a muon in $d\vec{\omega}$ striking $d\vec{s}$ produces an event of type $i;j,k$. The index i denotes the various types of scintillation-detector signals, similar to those described by Meyer *et al.*[11,12] The indices j,k represent the 16 possible combinations of vertical

TABLE III. Combinations of vertical and horizontal flash-tube signals with corresponding information on particle trajectory. θ is zenith angle, ξ is projected zenith angle, and φ is azimuth angle.

Vertical flash tubes $k=$		Horizontal flash tubes $j=1$ U	2 M	3 L	4 Gap in horizontal flash-tube array
1	α	θ	θ	θ	φ
2	β	θ	θ	θ	φ
3	γ	θ	θ	θ	φ
4	Gap in vertical flash-tube array	ξ	ξ	ξ	(No track)

and horizontal flash-tube elements which could be struck, as detailed in Table III.

Table III shows how nine combinations of the indices permit determination of the zenith angle θ, while the gaps in the system produce six combinations giving only partial information on the particle trajectory, as well as one combination giving no track information at all. In analyzing the combinations of flash-tube signals in this manner, there is an implicit summation over another index denoting the three vertical and three horizontal planes of flash tubes in a module (e.g., α in Table III denotes $\alpha_1, \alpha_2, \alpha_3$).

To approximate the evaluation of $dA_{i;j,k}/d\theta$, an average triggering efficiency $\langle\epsilon_t(\theta,\varphi)\rangle$ is calculated precisely. In this geometrical calculation, the effects of trajectories which clip the corners of the scintillators formed by the top and sides and the bottom and sides are included, although a similar small effect at the ends is neglected.

Effective regions for triggering the scintillation detector are then constructed by overlaying the projected areas of individual detectors appropriately weighted by the efficiency $\langle\epsilon_t(\theta,\varphi)\rangle$. For events involving two or more scintillators, account is taken of the fact that the effective threshold for observing pulses on the oscilloscope display is slightly lower than the trigger threshold. Accordingly, an additional overlay of the geometrical areas with an 8-MeV threshold is used for these events. Finally, the effective area of each flash-tube element is projected upon the effective scintillator regions to produce the differential apertures $dA_{i;j,k}/d\theta$. Included as a weighting factor in this calculation is the flash-tube detection efficiency $P_2(\xi)$ shown in Fig. 7. Thus the minimum requirement for recognizing a track projection is a scintillation-detector signal together with a display from at least two contiguous flash tubes in the two layers of an element. Figure 11(a) and 11(b) show various categories of differential apertures calculated in this way.

In order to verify the correctness of the complex and lengthy numerical calculations described above, an analytical analysis has been carried out[27] using linear combinations of the double-rail geometry formula [Eq. (A2)] of Jenkins,[28] which is based on a method due to Miyake.[29]

$$\frac{dA}{d\theta} = 4ab\left\{\sin^2\theta\left[1-\left(\frac{c/a}{\tan\theta}\right)^2\right]^{1/2} - \left(\frac{c}{a}\right)\sin\theta\cos\theta\cos^{-1}\left(\frac{c/a}{\tan\theta}\right)\right\}, \qquad \text{(A2)}$$

where

a = height of rectangular detectors,
b = length of rectangular detectors ($b \gg a, c$),
c = (horizontal) distance between the two detectors.

For $c \to 0$ (single-rail case),

$$\frac{dA}{d\theta} = 4ab\,\sin^2\theta\,. \qquad \text{(A2a)}$$

The coefficients giving the several classes of apertures in terms of the dimensions of the plane(s) of scintillation detectors and the multilayer sandwich of flash tubes are determined by Boolean logic analysis. In these calculations the effect of the checkerboard pattern of gaps in the several detector planes is taken account of by an "absorption coefficient" (a_s or a_{FT} = sensitive area/total rail area). This "checkerboard approximation" is seen to be tantamount to replacing the regular, fine-grained pattern of gaps which cause a_s and a_{FT} to be <1, with a random pattern. Figure 11 shows the good agreement between the precise numerical calculation and the simpler analytical method. The latter smoothes out the fine structure caused by the regular pattern of

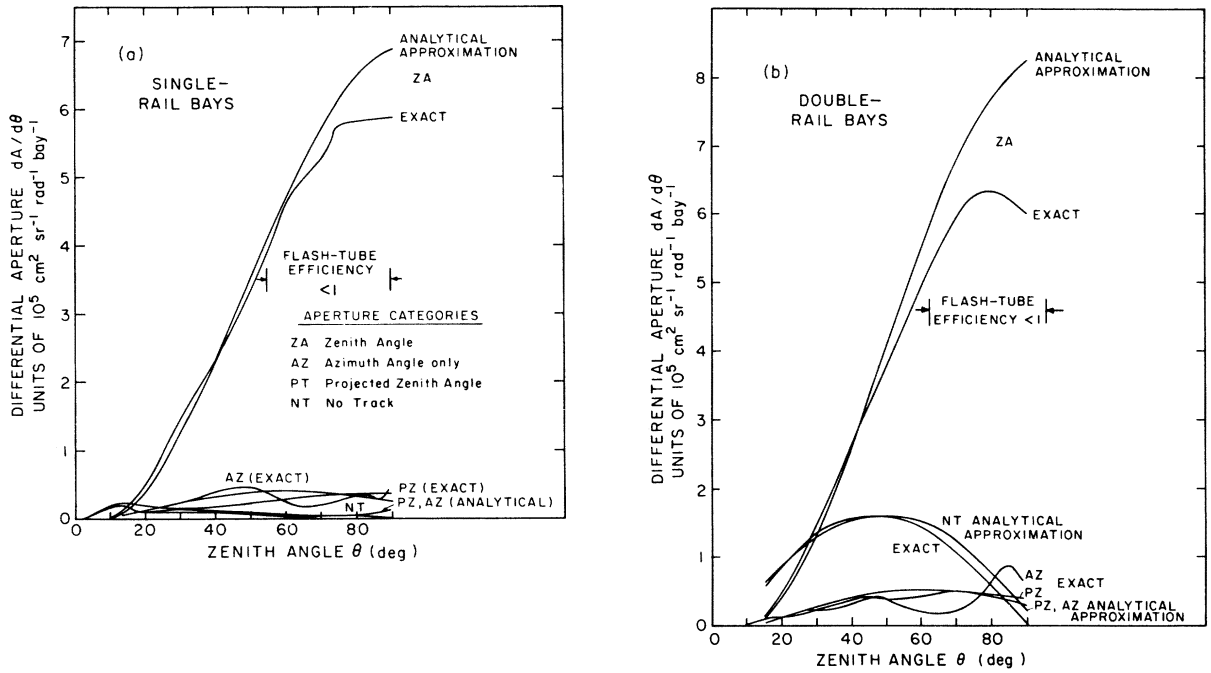

FIG. 11. Differential apertures (a) for single-rail bay detectors and (b) for double-rail bay detectors.

gaps, so that, in fact, the differences are qualitatively just as expected. The systematic differences in the region $60° < \theta < 90°$ reflect the fact that no flash-tube-efficiency correction has been made for the analytical calculations.

As noted earlier, based on operating experience as well as from a consideration of the data, monitoring of the equipment does not account for all of the inefficiencies in various sections of the flash-tube system. To evaluate exactly the effect of varying amounts of "excess inefficiency" on the apertures requires an excessive computational effort. However, for a relatively small excess inefficiency, it is possible to calculate the effect on the apertures using the analytic approach. In this approach we calculate the derivatives with respect to the absorption coefficient a_{FT} for the flash-tube array which describe the decrease in system aperture for determining the zenith angle of muons, and the corresponding increase in apertures for events which give at most partial data on muon trajectories. Thus apertures are corrected using an expression of the form

$$\left(\frac{dA}{d\theta}\right)_{\text{corr}} = \left(\frac{dA}{d\theta}\right)_{\text{exact}} \left[1 + F_{\text{anal}}(\theta)\frac{\Delta a_{FT}}{a_{FT}}\right], \qquad \text{(A3)}$$

where

$$F_{\text{anal}}(\theta) = \left(\frac{d\left(\frac{dA}{d\theta}\right)\Big/\frac{dA}{d\theta}}{da_{FT}/a_{FT}}\right)_{\text{anal}} . \qquad \text{(A4)}$$

Figure 12 shows the correction factors $F_{\text{anal}}(\theta)$

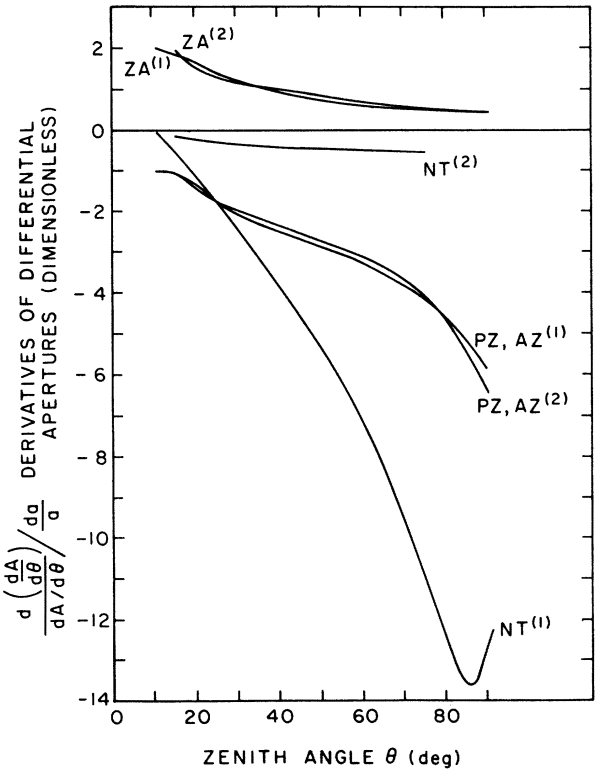

FIG. 12. Derivatives of differential apertures. (1) and (2) refer to single- and double-rail sections, respectively.

calculated for the several classes of apertures. Since events must fall into one of the listed categories, the derivatives satisfy a constraint equation

$$\sum d\frac{dA}{d\theta} = 0\,, \tag{A5}$$

where the sum extends over the four types of apertures. Analysis of the data indicates that $\Delta a_{FT}/a_{FT}$ has the value 0.16. For the largest apertures, denoted ZA in Figs. 11(a) and 11(b), the correction term $F_{anal}(\theta)(\Delta a_{FT}/a_{FT})$ is small ($\ll 1$). For the smallest aperture, denoted NT in Fig. 10(a), the correction is large (~1). However, NT/ZA is quite small (~$\frac{1}{20}$), and the fact that $\Delta a_{FT}/a_{FT}$ is small (~$\frac{1}{6}$) ensures that higher-order terms in Eq. (A3) are relatively unimportant. Accordingly it is concluded that the corrections in the apertures made with Eq. (A3) have sufficient accuracy for our purpose.

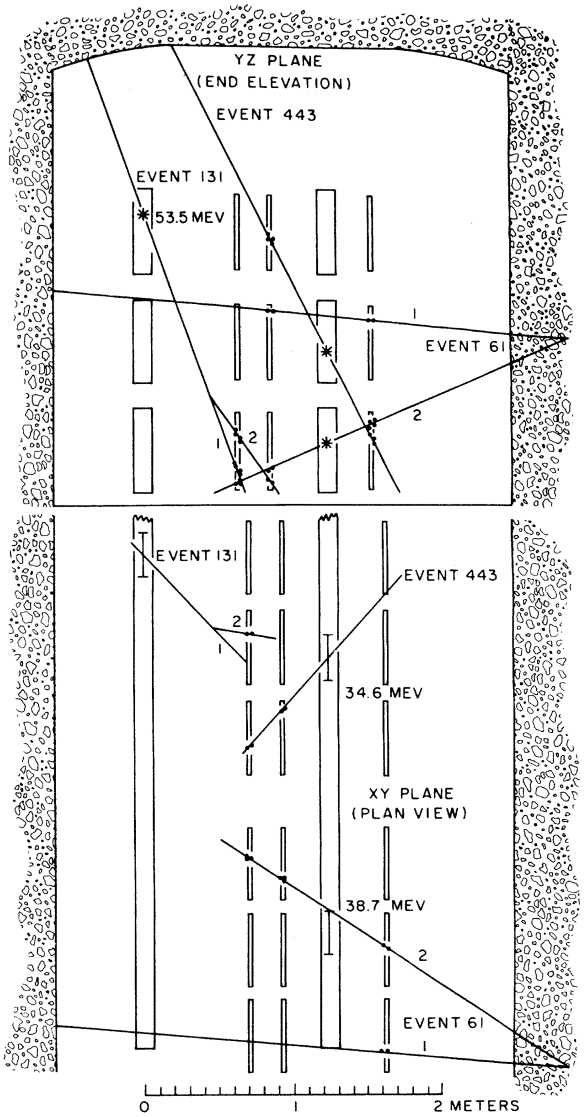

FIG. 13. Particle trajectories for three representative events.

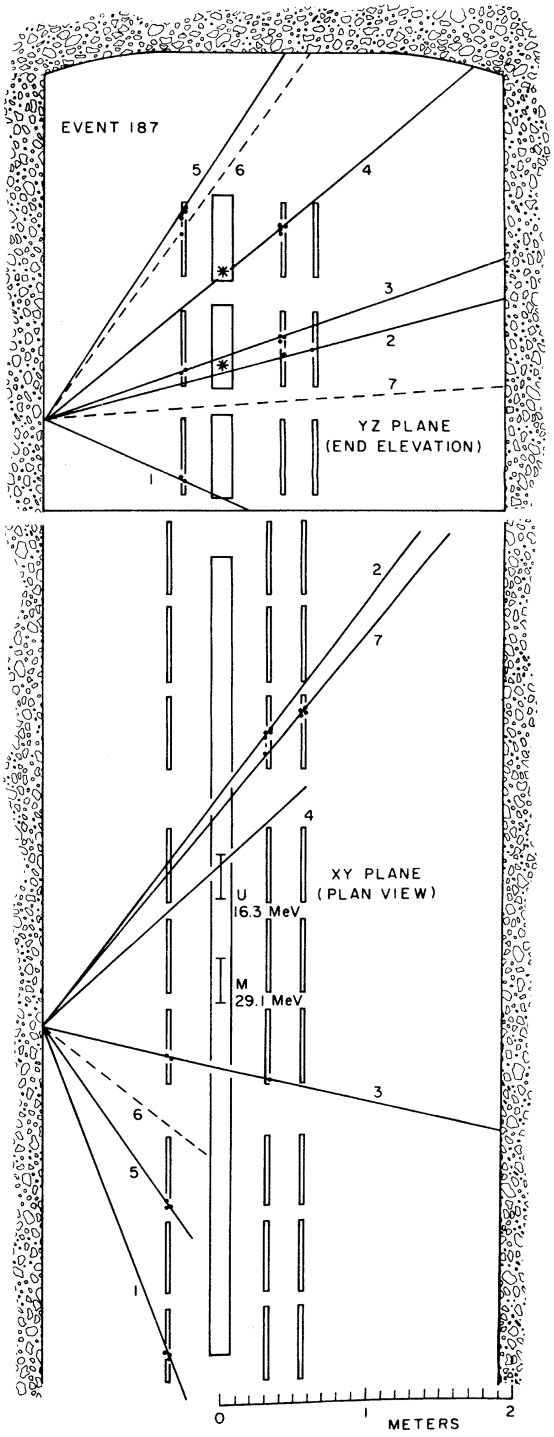

FIG. 14. Particle trajectories for a neutrino-induced interaction of unusual complexity.

APPENDIX B. DESCRIPTION OF REPRESENTATIVE EVENTS

Figure 13 shows three representative events (not simultaneous), superimposed on a single figure which shows the outlines of the detectors over a two-module region.

Event 131 has a zenith angle of $34° \pm 5°$, so that it is probably a pentrating cosmic-ray muon. This event is somewhat unusual in that it has a "vertex" in the air space of the tunnel. The vertex angle is 20.0°, so that if track 2 is a knock-on electron its energy is 7.7 MeV, which is not inconsistent with the ~10-MeV energy loss detected in the glass and aluminim flash-tube structure. The event position as determined from the scintillation-detector signals appears as an error bar in the xy plane, and the flash-tube signals appear as dots. The energy deposition in the scintillation detector is consistent with the oblique muon trajectory in the sensitive volume. The relatively small number of flash-tube signals is typical of events with small zenith angles.

Event 61, with two tracks having zenith angles of 68° and 84°, is clearly a neutrino-induced interaction. This is also an unusual event, with a vertex located at a distance of 0.27 ± 0.15 m inside the concrete lining of the tunnel. Had the vertex been deeper inside the rock it could have been an example of production of a W boson which decayed into a second muon. However, the event as reconstructed is probably an inelastic neutrino interaction. The absence of some flash-tube signals in the plan view of track 1 may indicate a particle which did not pentrate the full width of the tunnel, or it may indicate localized flash-tube inefficiency.

Event 443, with zenith angle of $41° \pm 2°$, is a single-particle event whose direction corresponds to the range where it is about equally likely to be a penetrating cosmic-ray muon or a neutrino-induced muon.

These events demonstrate the incomplete nature of trajectory data due to detector inefficiency which is partly geometrical and in certain cases partly physical.

Figure 14 shows the most complex event which was found to be amenable to detailed analysis. It is an interaction at the tunnel wall of an upward-going neutrino, which produces a large-angle shower of charged particles. Six or seven such particles, apparently aggregating a considerable transverse momentum, can be clearly determined to traverse a full scintillation-detector bay. For the analysis, scintillation-detector information, cluster patterns of flash-tube signals, and even likely gap effects are considered, though the latter must be invoked with extreme caution. The three dashed track fragments are somewhat speculative. The scintillation signal in the middle segment at an apparent distance 2.6 m from the end is seen to be caused by tracks 2 and 3 at distances of 2.0 m and 3.8 m.

In Figures 13 and 14 a few single flashes are suppressed for clarity. An average of five single flashes per module per event are observed, presumed due to background radioactivity. These stray flashes help to confirm during routine operation that the flash-tube pulsing and readout system is functioning correctly.

---

*Now at Space Sciences Laboratory, The Aerospace Corporation, Los Angeles, California 90009.

†Now at Beckman Instruments, Inc., Scientific Instruments Division, Irvine, California 92713.

‡Now at Lockheed Palo Alto Research Laboratory, Palo Alto, California 94304.

**Now at the University of Hong Kong, Department of Physics.

[1]F. Reines and J. P. F. Sellschop, Sci. Am. 214 (No. 2), 40 (1966).

[2]J. L. Osborne, S. S. Said, and A. W. Wolfendale, Proc. Phys. Soc. (London) 86, 93 (1965); J. L. Osborne, A. W. Wolfendale, and E. C. M. Young, in *Neutrino '72*, proceedings of the Euro-Physics Conference, Balatonfüred, Hungary, 1972, edited by A. Frenkel and G. Marx (OMKDK-TECHNOINFORM, Budapest, Hungary, 1972), Vol. 2, p. 233.

[3]S. Miyake, in *Proceedings of the Thirteenth International Conference on Cosmic Rays, Denver*, 1973 (Colorado Associated University Press, Boulder, 1973), p. 3638.

[4]Although the total quantity of liquid scintillator is only 20 metric tons, the long range of these muons causes a large volume of rock surrounding the detectors to function as an effective target for the interactions. Remarkably, the rate at which events are observed is equal to the interaction rate of cosmic-ray neutrinos in a rock target aggregating 800 tons, assuming that all interactions are detected with 100% efficiency.

[5]F. Reines, W. R. Kropp, H. W. Sobel, H. S. Gurr, J. F. Lathrop, M. F. Crouch, J. P. E. Sellschop, and B. S. Meyer, Phys. Rev. D 4, 80 (1971).

[6]M. R. Krishnaswamy, M. G. K. Menon, V. S. Narasimham, K. Hinotani, N. Ito, S. Miyake, J. L. Osborne, A. J. Parsons, and A. W. Wolfendale, Proc. R. Soc. (London) A323, 511 (1971). This group worked at the Kolar Gold Fields in India (KGF).

[7]M. F. Crouch, H. S. Gurr, A. A. Hruschka, T. L. Jenkins, W. R. Kropp, F. Reines, and H. W. Sobel, IEEE Trans. Nucl. Sci. NS-13, 424 (1966).

[8]M. F. Crouch, University of California, Irvine, Report No. UCI-10P19-20, 1969 (unpublished). M. Conversi and A. Gozzini, Nuovo Cimento 2, 189 (1955).

[9]The flash tubes were purchased from International Research and Development Co. Ltd., Newcastle upon Tyne, England. A. Robertshaw was Project Engineer.

[10]We have been unable to devise any technique for

monitoring the flash-tube system with ionizing radiation. The tracks of actual events play some monitoring role, but only serve to give occusional checks of small portions of the system. A few random flashes attributed to background radio activity are ordinarily seen in properly operating flash-tube modules, giving some indication of the degree of normalcy of the system, though offering no test of the important timing interrelationships for the system. The photoelectric readout circuits can be readily tested with a strong light source, since the photocell light shields are not completely opaque. Finally humidity monitors label periods when the relative humidity reaches levels at which experience shows the system operation to be undependable.

[11]The histogram takes into account, event by event, the uncertainty in the determination of the zenith angle, which ranges from ±1° to as high as ±15° in a few cases, the average being ±3.4°. We assume a normal distribution for probability vs angle for each event, so that one event may contribute a fraction of a count to more than one 5° angular bin in some cases. The resulting histogram of observed counts N_i, sometimes termed on "ideogram," therefore contains nonintegral numbers of events in most angular bins.

[12]A. Hald, *Statistical Theory with Engineering Applications* (Wiley, New York, 1952). Details of the iterative procedure using exact expressions for the likelihood functions in a similar calculation are given in Ref. 25.

[13]Expressions for muon energy loss may be found in A. Petrukhin, in *Proceedings of the 1976 DUMAND Summer Workshop, University of Hawaii, Honolulu*, edited by A. Roberts (Fermilab, Batavia, Ill., 1976), pp. 322ff.

[14]E. C. M. Young, private communication.

[15]Y. Pal, in Proceedings of Case Conference on the Interaction between Cosmic Rays and High Energy Physics, 1964 (unpublished).

[16]B. C. Barish *et al.*, Phys. Rev. Lett. 39, 1595 (1977).

[17]H. H. Chen, W. R. Kropp, H. W. Sobel, and F. Reines, Phys. Rev. D 4, 99 (1971).

[18]M. G. K. Menon and P. V. Ramana Murphy, in *Progress in Elementary Particle and Cosmic Ray Physics*, edited by J. G. Wilson and S. A. Wouthuysen (North-Holland, Amsterdam, 1967), Vol. IX, p. 163.

[19]B. C. Barish *et al.*, Phys. Rev. Lett. 40, 1414 (1978).

[20]B. C. Barish, Caltech Report No. CALT 68-621, 1977 (unpublished).

[21]S. Weinberg, Phys. Rev. Lett. 19, 1264 (1967).

[22]Since our results represent an integral over the neutrino energy spectrum [Eq. (5)], they do not verify the detailed shape of the spectrum. Our experiment was designed to determine the total intensity and angular variation of the underground muon flux and to compare the results with predictions. In the interest of simplicity in exploratory experiments we chose to detect the neutrinos via the muons produced by their interaction in the rock surrounding large-area detectors. These muons were counted when they penetrated the detectors. Accordingly, we did not ordinarily see the ν-reaction vertex nor did we obtain information as to the energy of the hadronic cascade or the muon (except that it was $\gtrsim$20 MeV). It does not seem feasible to instrument the mass of rock required ($\sim 10^8$ tons) to ensure detailed visibility of the event and obtain a counting rate great enough to make measurements at interesting energies ($>10^3$ GeV). An approach which obviates these shortcomings has been suggested by a group called DUMAND (Deep Underwater Muon and Neutrino Detector) which proposes to employ Cerenkov radiation in an undersea array. [*Proceedings of the 1976 DUMAND Summer Workshop, University of Hawaii, Honolulu* (Ref. 13)].

[23]The spectrum of extraterrestrial neutrinos is, in fact, expected to be less steep (up to a factor of E) than the atmospheric spectrum because there is no competition between absorption and decay of parent particles, e.g., K, π, μ.

[24]It was recently pointed out by D. Eichler (private communication) that our results bear on the cosmological question of deuterium production. If the observed deuterium was produced in the big bang, then in the standard cosmology, the baryon density of the universe must be much less than the closure density [R. V. Wagoner and D. N. Schramm, Annu. Rev. Nucl. Sci. 27, 37 (1977)]; the familiar "missing-mass" hypothesis generally requires that the deuterium be produced by more recent astrophysical processes. Thus there has been more discussion as to what astrophysical processes, if any, could produce deuterium at the observed level. R. Epstein, J. Lattimer, and D. N. Schramm [Nature (Lond.) 263, 198 (1976)] have argued against neutron capture, other than in the big bang, and star disruption models. They do allow spallation models with fast particles having initial energies in excess of 30 GeV and R. Epstein [Astrophys. J. 212, 595 (1977)] has proposed such a model. However, according to Eichler the neutrinos that are a by-product of the high-energy reactions in Epstein's model would have been detectable by our apparatus above the atmospheric background, unless they were red-shifted by a factor of at least 500. This is an interesting constraint, since galaxy formation and the ensuing production of high-energy particles is generally placed at a red shift less than 10. It should be noted that the value for this critical red shift depends on the spectrum assumed for the high-energy particles and hence for the resultant neutrinos; the factor 500 presumes a power-law tail with a differential spectral index of −2.6. However, assumptions regarding the spectrum could be obviated to a large extent by measuring the neutrino energy, as in Project DUMAND, for example.

[25]B. S. Meyer, J. P. F. Sellshop, M. F. Crouch, W. R. Kropp, H. W. Sobel, H. S. Gurr, J. F. Lathrop, and F. Reines, Phys. Rev. D 1, 2229 (1970).

[26]B. S. Meyer, Ph. D. thesis, University of the Witwatersrand, 1969 (unpublished); F. Reines, M. F. Crouch, T. L. Jenkins, W. R. Kropp, H. S. Gurr, G. R. Smith, J. P. F. Sellschop, and B. Meyer, Phys. Rev. Lett. 15, 551 (1965).

[27]M. F. Crouch, University of California, Irvine, Report No. UCI-10P19-116, 1976 (unpublished).

[28]T. L. Jenkins, private communication.

[29]S. Miyake, private communication.

[30]D. E. Groom, J. W. Keuffel, and J. L. Morrison, University of Utah, private communication, 1977.

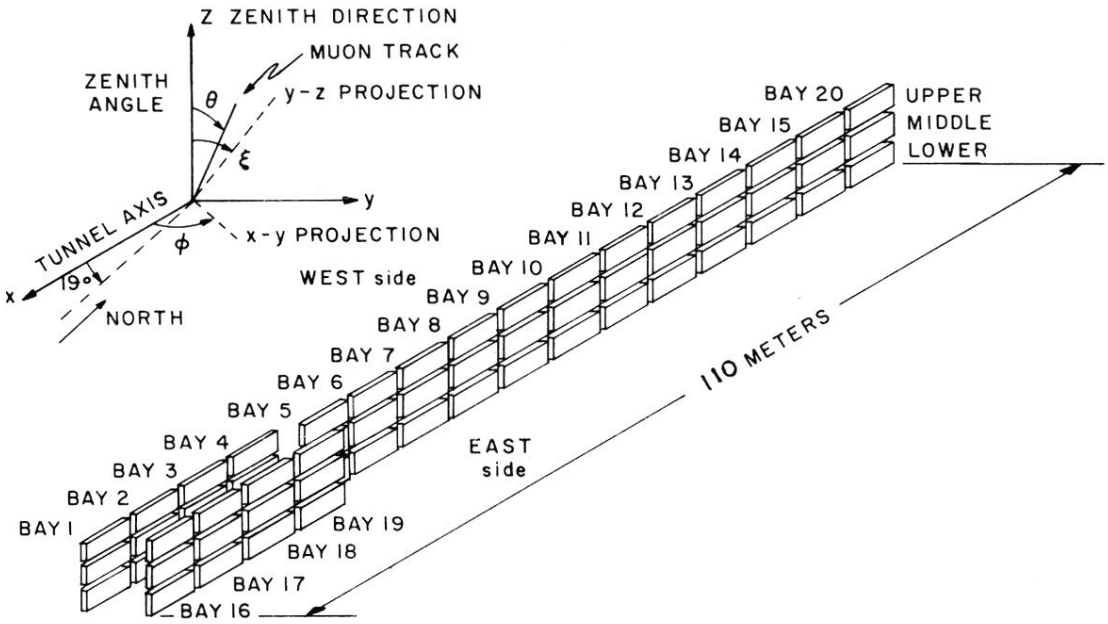

FIG. 1. The scintillation-detector array and the angular coordinate system.

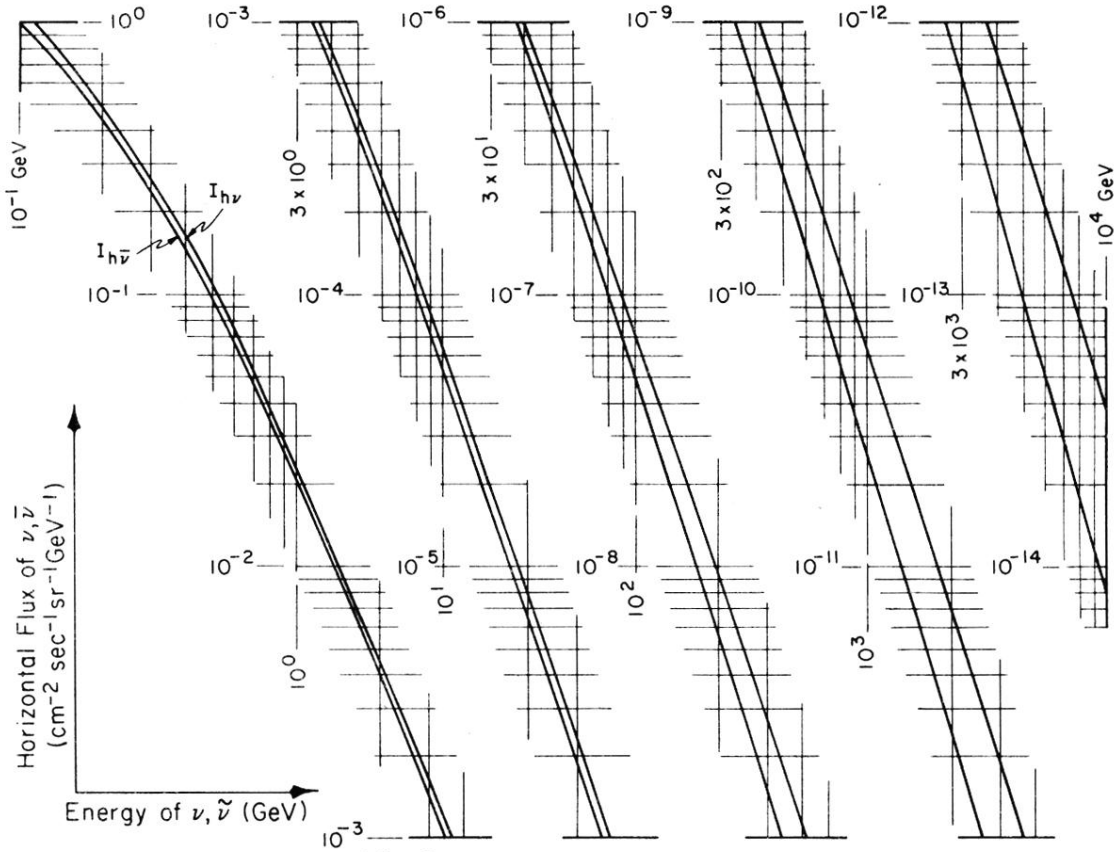

FIG. 10. Horizontal flux for cosmic-ray muon neutrinos, muon antineutrinos.

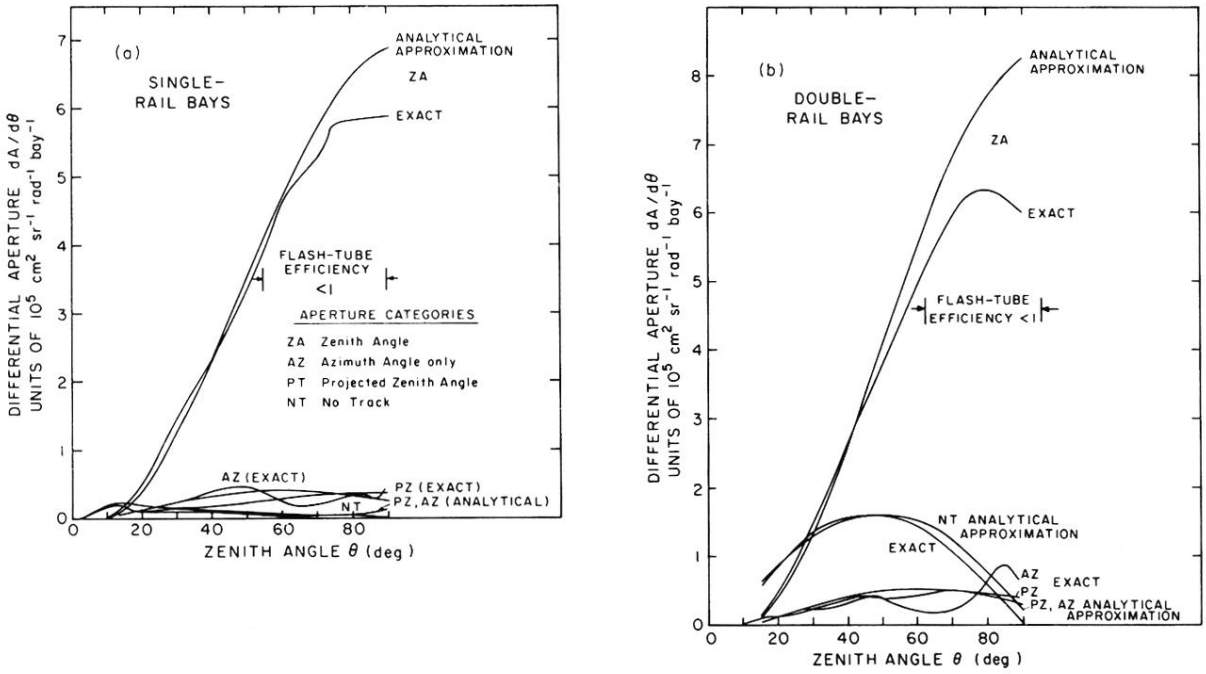

FIG. 11. Differential apertures (a) for single-rail bay detectors and (b) for double-rail bay detectors.

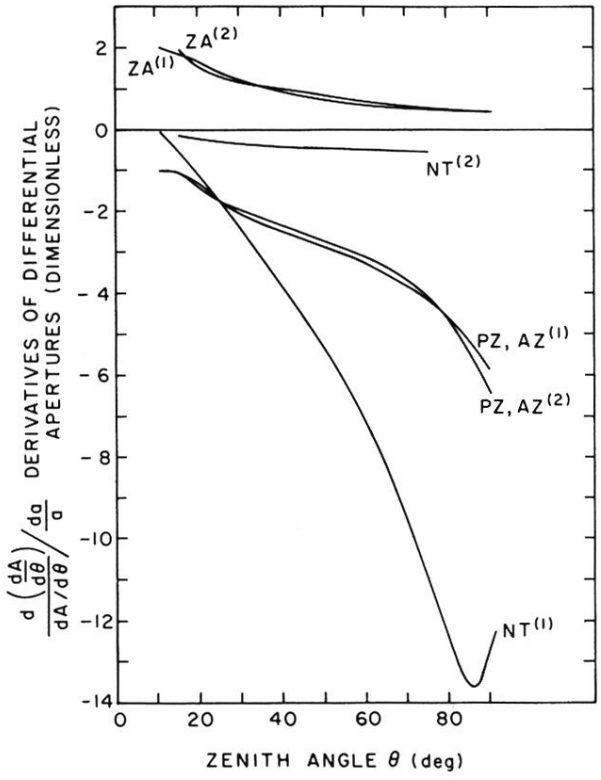

FIG. 12. Derivatives of differential apertures. (1) and (2) refer to single- and double-rail sections, respectively.

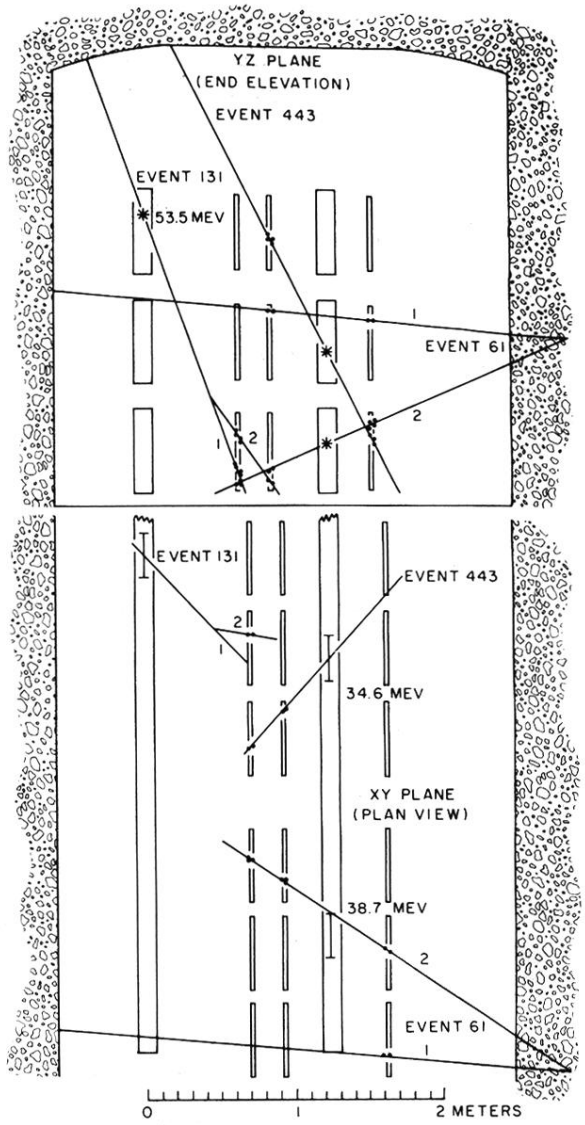

FIG. 13. Particle trajectories for three representative events.

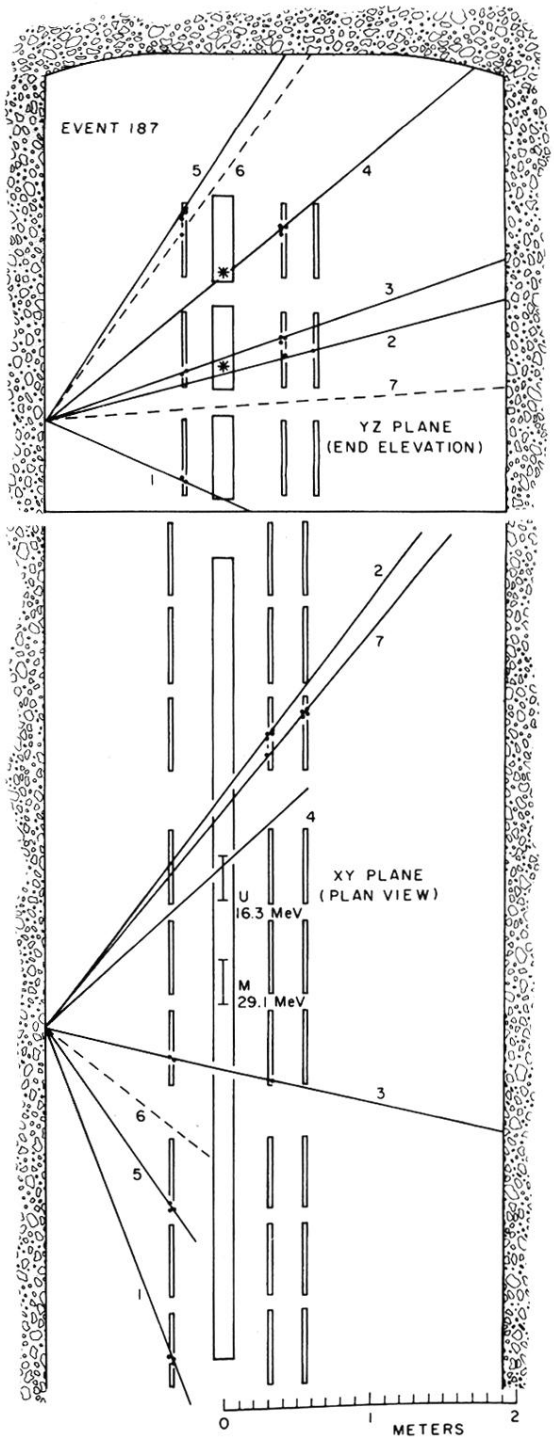

FIG. 14. Particle trajectories for a neutrino-induced interaction of unusual complexity.

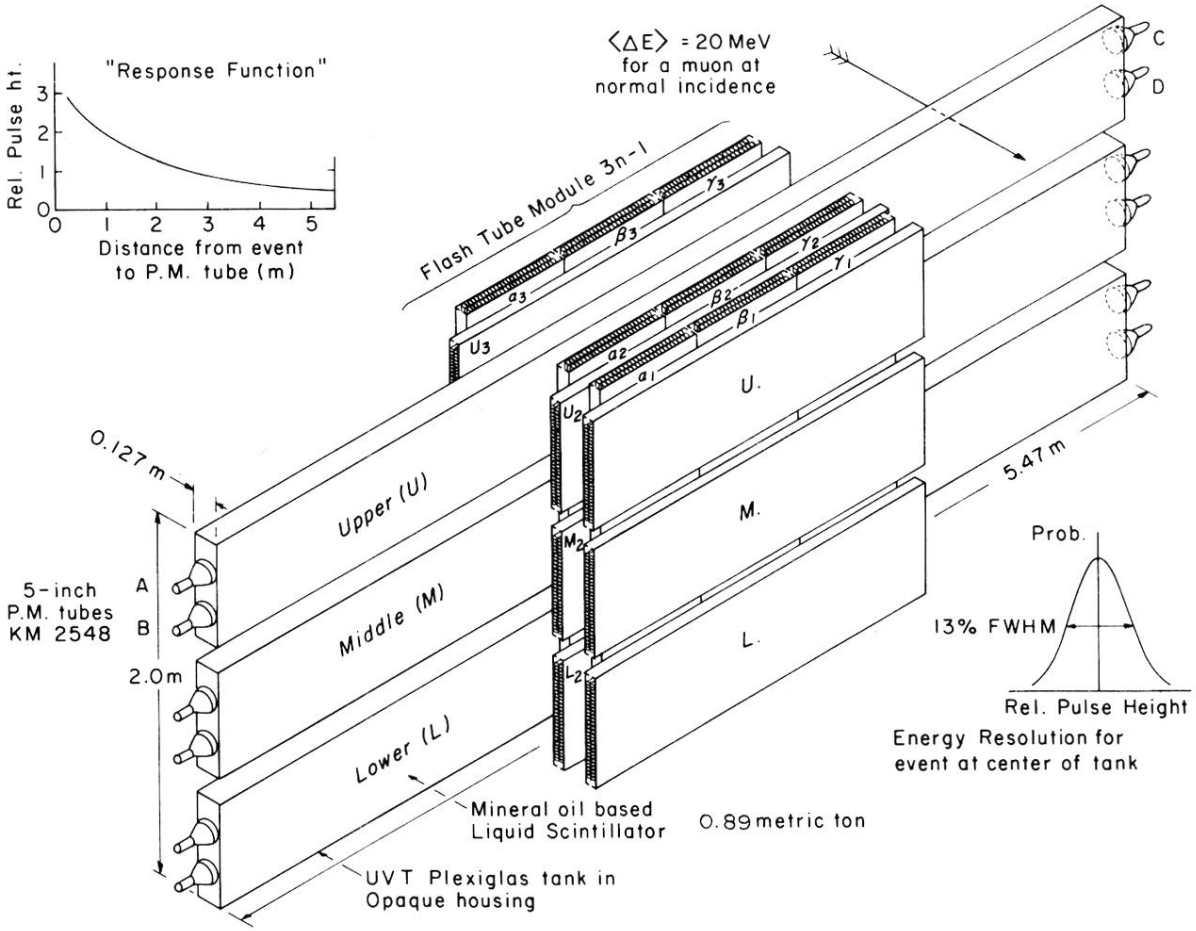

FIG. 2. Details of the nth scintillator bay and the $(3n-1)$st flash-tube module.

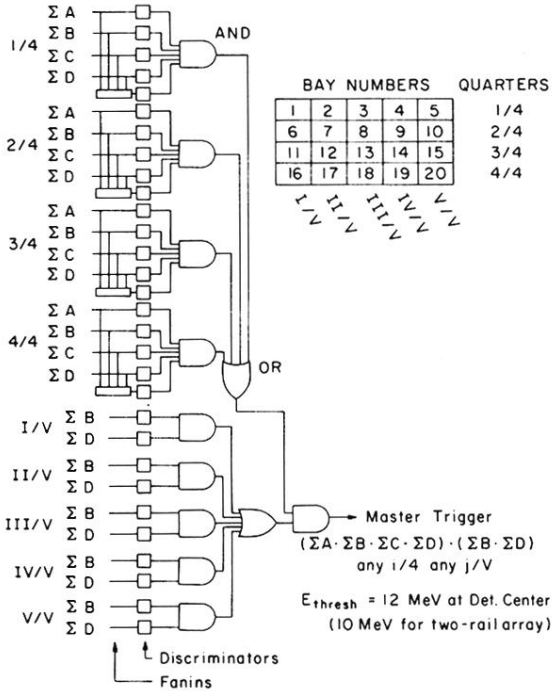

FIG. 3. Logic circuits for triggering the scintillation-detector array.

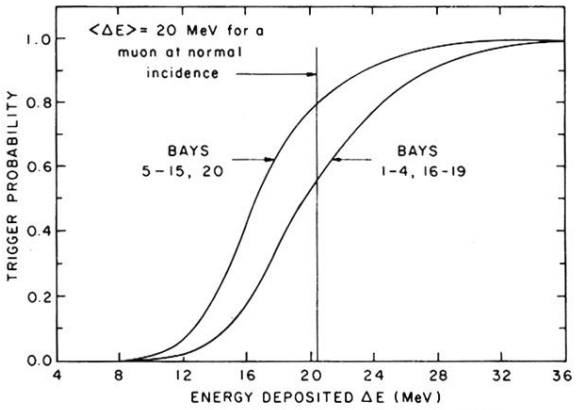

FIG. 4. Triggering probability for the scintillation-detector array vs energy deposition.

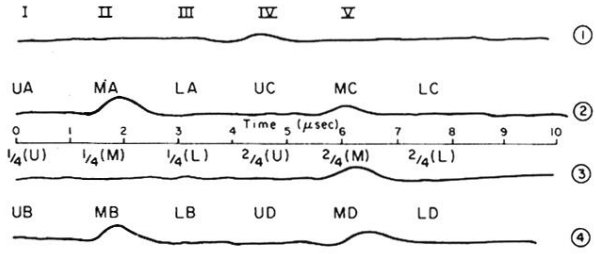

First-Half Chronotron Display: Event No. 205 - BAY 9, Middle Tank.

FIG. 5. Pulse-position code for scintillation-detector signals, showing a representative event—event No. 205, middle detector, bay 9.

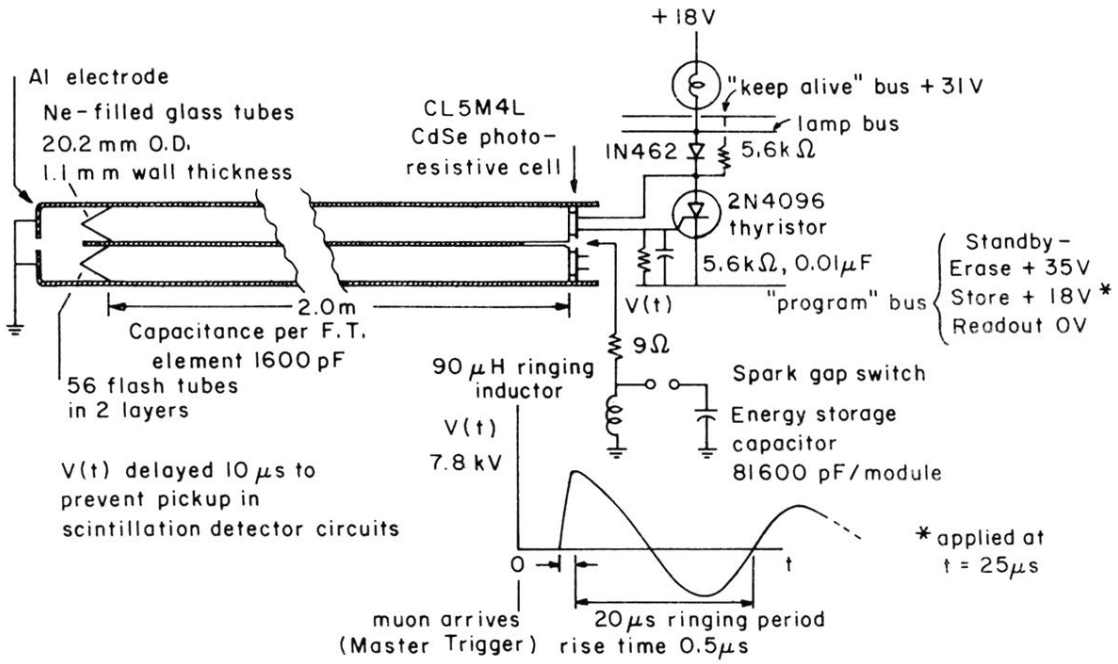

FIG. 6. Flash-tube element and associated circuits.

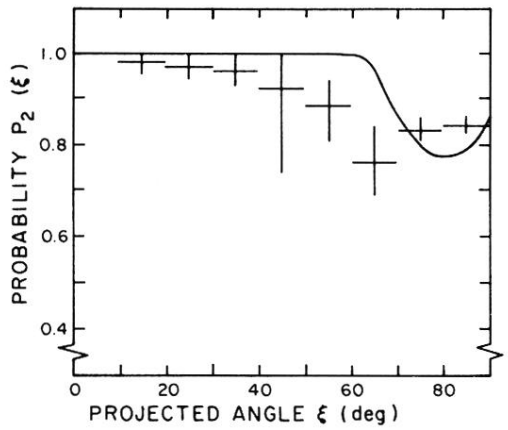

FIG. 7. Probability $P_2(\xi)$ of a two-layer response in a flash-tube element vs projected angle ξ for horizontal flash tubes or φ for vertical tubes.

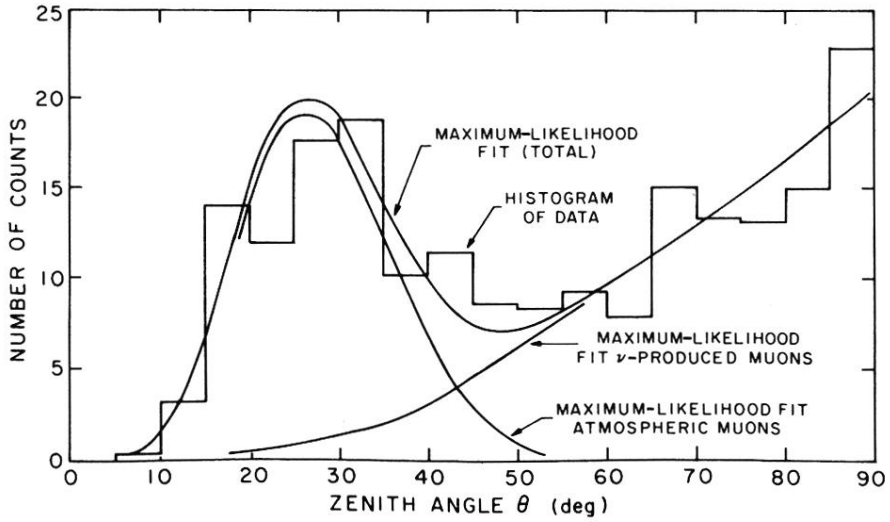

FIG. 8. Observed and expected numbers of counts vs zenith angle for events in which zenith angle is determined.

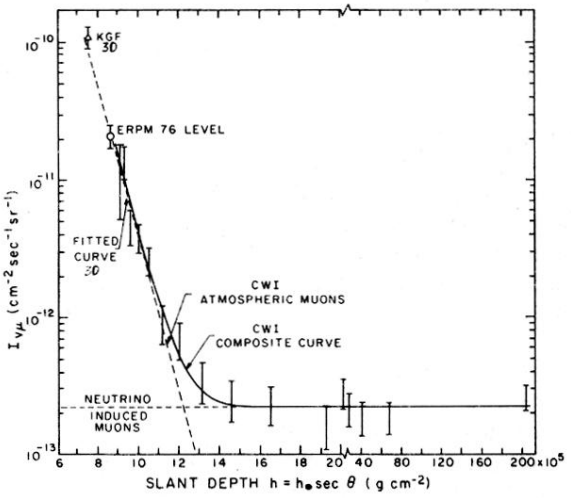

FIG. 9. Vertical intensity $I_{\nu\mu}$ of muons vs slant depth h, deduced from muon angular distribution at $h_0 = 8.89 \times 10^5$ g cm^{-2}. Fitted curve is from Ref. 30.